12-2017

Human Metapneumovirus Induces Formation of Inclusion Bodies for Efficient Genome Replication and Transcription

Nicolás P. Cifuentes-Muñoz
University of Kentucky, ncifuentes@uky.edu

Jean Branttie
University of Kentucky, jean.branttie@uky.edu

Kerri Beth Slaughter
University of Kentucky, kerri.slaughter@uky.edu

Rebecca Ellis Dutch
University of Kentucky, rebecca.dutch@uky.edu

Human Metapneumovirus Induces Formation of Inclusion Bodies for Efficient Genome Replication and Transcription

Notes/Citation Information
Published in *Journal of Virology*, v. 91, issue 24, e01282-17, p. 1-18.

Digital Object Identifier (DOI)
https://doi.org/10.1128/JVI.01282-17

AMERICAN SOCIETY FOR MICROBIOLOGY | Journal of Virology®

GENOME REPLICATION AND REGULATION OF VIRAL GENE EXPRESSION

Human Metapneumovirus Induces Formation of Inclusion Bodies for Efficient Genome Replication and Transcription

Nicolás Cifuentes-Muñoz, Jean Branttie, Kerri Beth Slaughter, Rebecca Ellis Dutch

Department of Molecular and Cellular Biochemistry, University of Kentucky College of Medicine, Lexington, Kentucky, USA

ABSTRACT Human metapneumovirus (HMPV) causes significant upper and lower respiratory disease in all age groups worldwide. The virus possesses a negative-sense single-stranded RNA genome of approximately 13.3 kb encapsidated by multiple copies of the nucleoprotein (N), giving rise to helical nucleocapsids. In addition, copies of the phosphoprotein (P) and the large RNA polymerase (L) decorate the viral nucleocapsids. After viral attachment, endocytosis, and fusion mediated by the viral glycoproteins, HMPV nucleocapsids are released into the cell cytoplasm. To visualize the subsequent steps of genome transcription and replication, a fluorescence *in situ* hybridization (FISH) protocol was established to detect different viral RNA subpopulations in infected cells. The FISH probes were specific for detection of HMPV positive-sense RNA (+RNA) and viral genomic RNA (vRNA). Time course analysis of human bronchial epithelial BEAS-2B cells infected with HMPV revealed the formation of inclusion bodies (IBs) from early times postinfection. HMPV IBs were shown to be cytoplasmic sites of active transcription and replication, with the translation of viral proteins being closely associated. Inclusion body formation was consistent with an actin-dependent coalescence of multiple early replicative sites. Time course quantitative reverse transcription-PCR analysis suggested that the coalescence of inclusion bodies is a strategy to efficiently replicate and transcribe the viral genome. These results provide a better understanding of the steps following HMPV entry and have important clinical implications.

IMPORTANCE Human metapneumovirus (HMPV) is a recently discovered pathogen that affects human populations of all ages worldwide. Reinfections are common throughout life, but no vaccines or antiviral treatments are currently available. In this work, a spatiotemporal analysis of HMPV replication and transcription in bronchial epithelial cell-derived immortal cells was performed. HMPV was shown to induce the formation of large cytoplasmic granules, named inclusion bodies, for genome replication and transcription. Unlike other cytoplasmic structures, such as stress granules and processing bodies, inclusion bodies are exclusively present in infected cells and contain HMPV RNA and proteins to more efficiently transcribe and replicate the viral genome. Though inclusion body formation is nuanced, it corresponds to a more generalized strategy used by different viruses, including filoviruses and rhabdoviruses, for genome transcription and replication. Thus, an understanding of inclusion body formation is crucial for the discovery of innovative therapeutic targets.

KEYWORDS HMPV, pneumovirus, inclusion bodies, replication

Received 26 July 2017 **Accepted** 25 September 2017

Accepted manuscript posted online 4 October 2017

Citation Cifuentes-Muñoz N, Branttie J, Slaughter KB, Dutch RE. 2017. Human metapneumovirus induces formation of inclusion bodies for efficient genome replication and transcription. J Virol 91:e01282-17. https://doi.org/10.1128/JVI.01282-17.

Editor Terence S. Dermody, University of Pittsburgh School of Medicine

Address correspondence to Rebecca Ellis Dutch, rdutc2@uky.edu.

Human metapneumovirus (HMPV) is a pathogen that affects all age groups worldwide, with an increased risk of severe disease being found in immunocompromised individuals, children under the age of 5 years, and the elderly (1–4). Together

with respiratory syncytial virus (RSV), HMPV belongs to the recently created *Pneumoviridae* family (5). HMPV infections account for an estimated 10% of respiratory tract infections and have incidence rates comparable to those of influenza virus infections during winter (3, 6). Nonetheless, no specific antiviral drugs or vaccines that protect from infections caused by HMPV are currently available, and clinical treatment is mainly supportive.

The virus genome is composed of a negative-sense single-stranded RNA of approximately 13.3 kb in size which encodes eight genes in the following order: 3′-N-P-M-F-M2-SH-G-L-5′ (2). The genome is encapsidated by multiple copies of the nucleoprotein (N) to give rise to helical nucleocapsids (7). Additionally, copies of the phosphoprotein (P) interact with N and recruit the L protein, an RNA-dependent RNA polymerase, and the cofactor M2-1 to the viral nucleocapsids (8–11). Estimates for Sendai virus, a paramyxovirus, show that a virion can contain up to 2,600 copies of N, 300 copies of P, and 50 copies of the L protein (12). After the viral glycoproteins mediate the steps of attachment, clathrin-mediated endocytosis, and virus-cell membrane fusion, nucleocapsids are released into the cell cytoplasm (13, 14). While few studies have examined HMPV replication, analogy to related viruses suggests that once in the cytoplasm, the viral RNA polymerase and its associated cofactors utilize viral genomic RNA (vRNA) as a template to transcribe viral mRNAs and to replicate more copies of the vRNA for the assembly of new particles (15). Replication of the vRNA is achieved through synthesis of a full-length positive-sense antigenome copy, or cRNA (15). The promoter signals that control viral replication, the leader (le) and trailer (tr), are located at the 3′ and 5′ ends of the genome, respectively. Additionally, other *cis*-acting elements within the genome are involved in the transcription of the eight individual HMPV genes, along with the mRNA capping and polyadenylation processes (15, 16). Though much progress in our understanding of HMPV entry has been made, important questions about replication and transcription remain to be elucidated. Furthermore, although different models have been proposed, the mechanism by which the viral RNA polymerase hypothetically changes from a transcriptional mode to a replicative mode is still not understood (17).

A number of nonsegmented negative-sense RNA (NNS) viruses from different families induce the formation of well-defined spherical cytoplasmic structures known as inclusion bodies (IBs) in infected cells. Viral components, such as genomic RNA and the N, P, and L proteins, are concentrated within these sites, likely for efficient genome replication and transcription. One of the earliest examples of inclusions found in the literature are Negri bodies, found in the cytoplasm of nerve cells infected by rabies virus (RABV) (18). Negri bodies range in size from 2 to 10 μm, and studies have reported the presence of the rabies virus genome, antigenome, and viral mRNAs within these structures (19). Interestingly, these bodies are initially not membrane bound, but they become surrounded by rough endoplasmic reticulum (RER) membranes as infection progresses (19). Another rhabdovirus, vesicular stomatitis virus (VSV), also induces the formation of cytoplasmic bodies for replication and transcription of the genome, but a cellular membrane association was not found (20). Inclusion body formation also seems to be a hallmark of filovirus replication (21, 22). Helical nucleocapsids within IBs closely associated with the membranes of the endoplasmic reticulum (ER) have been observed in Marburg virus-infected cells (22). From the replication bodies, Marburg and Ebola virus nucleocapsids were observed to be transported to budding sites, a process dependent on actin polymerization (23, 24). For some paramyxoviruses, the formation of IBs in infected cells was demonstrated many years ago by electron microscopy studies (25–28). Nucleocapsids were found within these non-membrane-bound bodies, and therefore, they were proposed to be viral replicative sites. For members of the *Pneumoviridae*, inclusion body formation upon infection or coexpression of the N and P proteins has been reported (8, 29, 30).

In the present work, we established a fluorescence *in situ* hybridization (FISH) protocol that permits detection of HMPV genomic, antigenomic, and mRNAs. Combining FISH with immunofluorescence and confocal three-dimensional (3D) reconstruc-

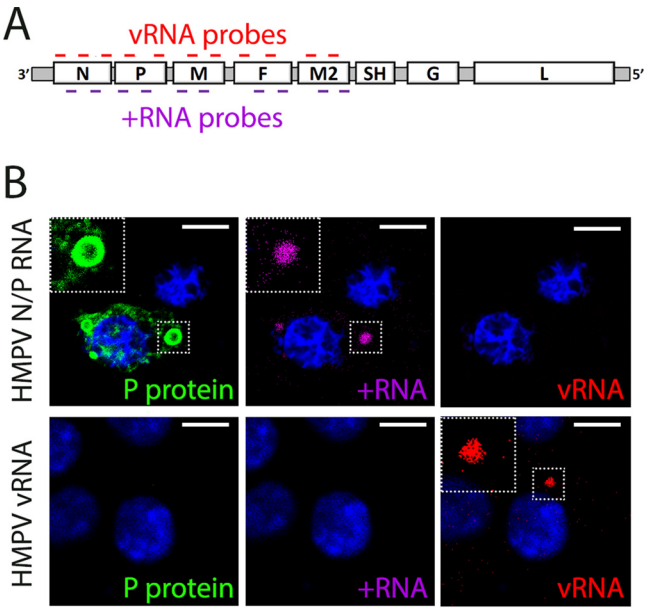

FIG 1 HMPV FISH probes are specific. (A) Schematic of the FISH probes designed for the present work. Probes span half of the genome, including the genes for N, P, M, F, and M2. The two sets of probes target the vRNA and the +RNA sequences, in red and purple, respectively. (B) BSR cells were transfected to express either HMPV N and P mRNAs (top) or the HMPV full-length genome (bottom) of strain JPS02-76 under the control of the T7 promoter. At 48 h posttransfection, cells were processed for FISH to detect vRNA (red) and +RNA (purple) and for immunofluorescence to detect the P protein (green). (Insets) Enlarged images of the small squares with dotted outlines. Bars, 10 μm.

tions, we imaged HMPV replication and transcription immediately after cell entry. HMPV replication and transcription occur, as for other NNS viruses, in well-defined spherical cytoplasmic IBs. HMPV IBs were predominantly located close to the cell nuclei and were distinct from other cytoplasmic structures, such as stress granules (SGs) or processing bodies (P bodies). Surprisingly, HMPV inclusion bodies were maintained at very low numbers, independent of the multiplicity of infection (MOI) used. Disruption of actin polymerization in infected cells allowed us to identify a role for actin polymerization in IB formation. Our results support a model in which IB formation was the result of the coalescence of multiple individual replicative sites. Using quantitative reverse transcription-PCR (RT-qPCR), we demonstrated that disruption of IB coalescence correlated with the less efficient replication and transcription of the viral genome at early times postinfection. These results broaden our current understanding of HMPV replication and also have important clinical implications, such as for the discovery of novel antiviral therapeutics.

RESULTS

Design and specificity of FISH probes. The processes of replication and transcription of the HMPV genome ultimately result in the synthesis of at least three different viral RNA species: full-length negative-sense vRNAs, full-length positive-sense antigenomic RNAs (cRNAs), and 8 subgenomic capped polyadenylated viral mRNAs (15). In our design, two independent sets containing 48 probes each were synthesized to perform FISH. One set of probes targeted the vRNA sequence, and the second set targeted the viral positive-sense RNA (+RNA) sequences in the region between nucleotides 1 and 5467. This region contains the genes for N, P, M, F, and M2, which are some of the genes most highly conserved between different HMPV strains (16). Thus, our probes could theoretically be used to detect multiple viral strains. We corroborated *in silico* that none of the probes from one set was complementary with probes from the other set. Therefore, the two probe sets detect different regions in either the vRNA or the +RNA sequence (Fig. 1A). However, the set of probes designed to target the

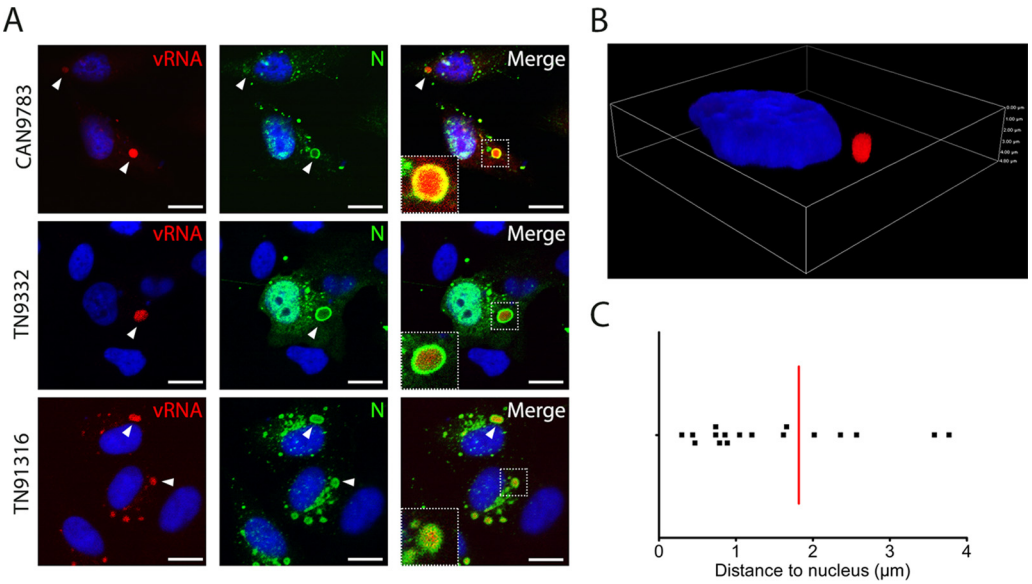

FIG 2 Inclusion body formation is a hallmark of HMPV infection. (A) BEAS-2B cells were infected with HMPV, fixed at 24 hpi (strain CAN97-83) or 72 hpi (strains TN9332 and TN9316), and processed for detection of vRNA (red) and the N protein (green). (Insets) Enlarged images of the small squares with dotted outlines. Bars, 10 μm. (B) Z-stack analysis of a cell infected with HMPV CAN97-83, showing an inclusion body (red) close to the cell nucleus (blue) at 24 hpi. (C) BEAS-2B cells were infected with HMPV CAN97-83, and at 24 hpi the distance between the IBs and the cell nuclei was measured using Z-stack analysis of 17 cells. The red bar indicates the average distance to the nucleus.

positive-sense RNA would potentially detect two species of viral RNAs: cRNAs and mRNAs. To determine the specificity of the two probe sets, we expressed the full-length vRNA or, alternatively, the HMPV N and P mRNAs from HMPV strain JPS0762 in BSR cells by transfection of the respective plasmids. The cells were processed for both FISH and immunofluorescence at 48 h posttransfection. Detection of HMPV N and P mRNAs was achieved with the set of probes designed for +RNA detection but not with the set designed for vRNA detection (Fig. 1B, top). The viral P protein was also assessed in these cells. Some of the P protein was found to be part of ring-shaped inclusion body-like structures that contained the signal for +RNAs. The formation of inclusion bodies after coexpression of the HMPV N and P proteins was previously reported (8); however, the presence of viral mRNA within these structures is a novel finding. On the other hand, detection of full-length vRNA was achieved using only the respective FISH probes (Fig. 1B, bottom). The vRNA signal was present in well-localized punctate cytoplasmic sites, even in the absence of other viral components. Thus, the results demonstrate that the sets of probes are specific for detection of HMPV +RNA and vRNA and that they can be used to detect sequences from other strains of HMPV besides CAN97-83.

HMPV induces formation of cytoplasmic inclusion bodies. After membrane fusion occurs in endosomal compartments (13), HMPV nucleocapsids are released into the cell cytoplasm to initiate viral replication and transcription. Early electron microscopy studies with viruses from the *Paramyxoviridae* family demonstrated the formation of inclusion bodies in the cell cytoplasm or even the nuclei of infected cells (25–28). For RSV, the formation of cytoplasmic inclusion bodies was reported upon infection of Vero cells (29). Furthermore, the N and P proteins have been identified to be the minimal components necessary for the assembly of both HMPV and RSV inclusion bodies (8, 30). In order to analyze IB formation by HMPV in a physiologically relevant cell line, human bronchial epithelial BEAS-2B cells were infected with different HMPV strains: the prototype strain CAN97-83 and two clinical isolates, TN9332 and TN91316. Infected cells were then fixed and processed for FISH using probes that target the vRNA (red) and for immunofluorescence using antibodies that detect the N protein (green). As expected, the vRNA and N signals colocalized in cytoplasmic IBs in infected cells (Fig. 2A, arrowheads). IBs were clearly observable by 24 h postinfection (hpi) for strain CAN97-83

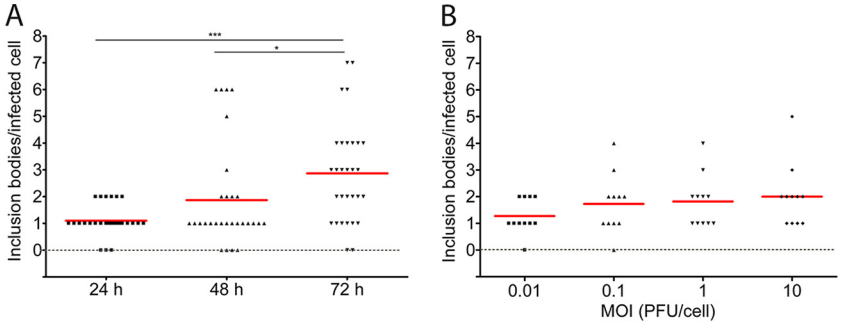

FIG 3 HMPV inclusion bodies are maintained at low numbers. (A) BEAS-2B cells were infected with rgHMPV CAN97-83 at an MOI of 1 PFU/cell, and cells were processed for FISH and immunofluorescence at 24, 48, and 72 hpi. (B) BEAS-2B cells were infected with rgHMPV CAN97-83 at different MOIs, and the cells were processed for FISH and immunofluorescence at 24 hpi. An inclusion body was counted as a vRNA-positive/N-positive perinuclear structure $\geq$0.5 μm in size. Student's *t* test was performed for statistical analysis. *, $P < 0.01$; ***, $P < 0.0001$. Red lines indicate the average number of inclusion bodies per infected cell.

but were evident only at later times postinfection for strains TN9332 and TN91316. The strongest N protein signal in the inclusion bodies was similar to that in cells coexpressing N and P, forming a ring structure around the RNA. HMPV inclusion bodies were always found to be cytoplasmic, and in most cases they were located very close to the nucleus. A 3D analysis of HMPV-infected cells using Z-stack imaging demonstrated that the average distance, edge to edge, between inclusion bodies and the nuclei was approximately 2 μm (Fig. 2B and C). Although the presence of vRNA associated with cytoplasmic IBs was recently reported for RSV (31), this is, to our knowledge, the first demonstration of the presence of vRNA in IBs in HMPV-infected cells.

HMPV-induced inclusion bodies are maintained at low numbers. Different viral RNA species synthesized during viral replication can be recognized by proteins of the innate immune system and induce the interferon (IFN) response (32). For the paramyxovirus parainfluenzavirus 5 (PIV5), it has been suggested that cytoplasmic IBs might represent a viral strategy to replicate the vRNA while circumventing the IFN cellular response (33). Interestingly, IBs were found to be kept at very low numbers in HMPV-infected cells. To quantitatively address this notion, two distinct experiments were performed. First, the number of inclusion bodies in infected cells was analyzed at late times postinfection. As a reference, the release of HMPV CAN97-83 infectious particles is initially detected by 12 hpi (34). Thus, BEAS-2B cells were infected with HMPV and fixed at 24, 48, and 72 hpi. Using FISH combined with immunofluorescence, vRNA-positive/N-positive perinuclear structures $\geq$0.5 μm in size were counted. A slight yet significant increase in the number of inclusion bodies was found from 24 to 72 hpi (Fig. 3A), with an average of approximately three IBs per infected cell being found at 72 hpi. The number of inclusion bodies was found to be up to seven in a single infected cell, but cells with more IBs were not found, suggesting that HMPV IBs are preferentially maintained at low numbers, generally between one and three. A second analysis was performed using different multiplicities of infection with cells fixed at 24 hpi. Surprisingly, in cells infected at an MOI as low as 0.01 PFU/cell, the number of inclusion bodies per infected cell did not significantly differ from the number per infected cell for cells infected at higher MOIs, such as 1 or even 10 PFU/cell (Fig. 3B). This result differs from what has been reported for RSV, in which up to 80 IBs per infected cell were observed (31).

Viral components of HMPV inclusion bodies. The nucleocapsid protein is an RNA-binding protein that coats the vRNA and the cRNA, giving rise to helical nucleocapsids that are used as the templates for genome replication and transcription (7, 15). Initial electron microscopic images of the inclusion bodies induced by paramyxoviruses showed an accumulation of nucleocapsids within these structures, suggesting that the IBs may serve as active replicative sites (25, 26, 28). The formation of inclusion body-like

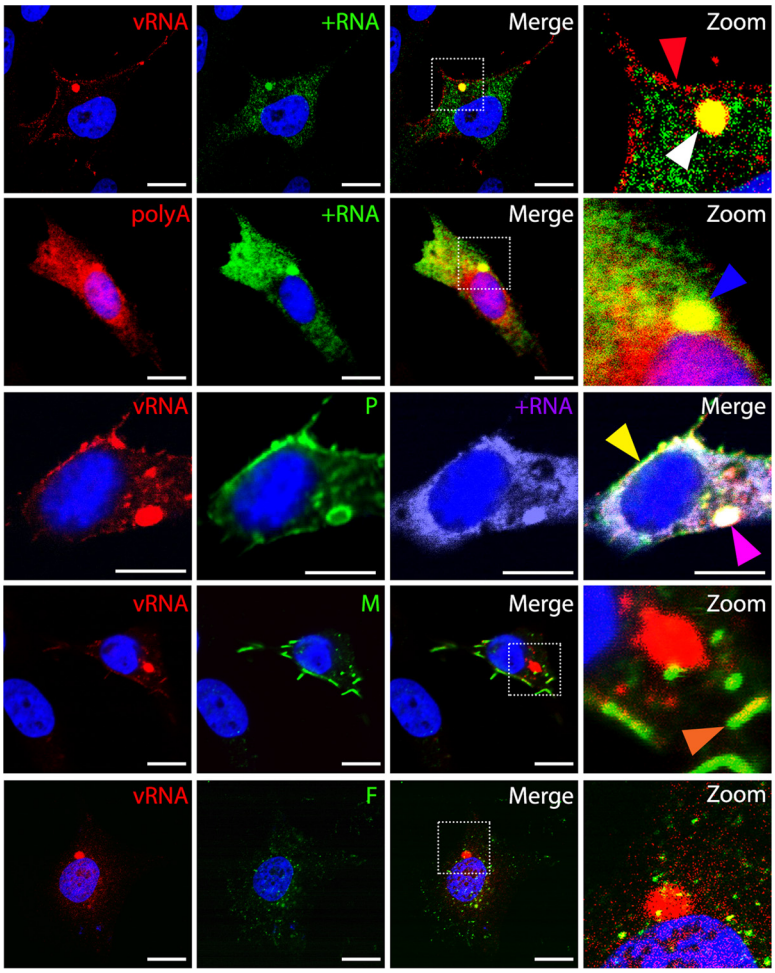

FIG 4 Inclusion bodies are sites of replication and transcription but not assembly. BEAS-2B cells were infected with HMPV CAN97-83 at an MOI of 3 PFU/cell and fixed at 24 hpi. FISH and immunofluorescence were performed to detect vRNA (red), +RNA (purple; green as a pseudocolor), polyadenylated RNAs (red), and the HMPV P, M, and F proteins (green). Bars, 10 μm. The squares with dotted outlines are magnified and shown as the zoom images in the right column.

structures has been demonstrated by coexpression of the N and P proteins of HMPV (8) as well as those of RSV (30), which suggests that in the absence of viral genomes, both proteins can fulfill an uncharacterized structural role in the formation of IBs. However, only recently has the presence of RSV and PIV5 vRNA in IBs been described (31, 33). Thus, we used FISH and immunofluorescence to identify other viral components present in IBs besides vRNA and the nucleoprotein. First, BEAS-2B-infected cells were simultaneously incubated with the two sets of FISH probes. A strong signal was detected for vRNA and +RNA colocalizing in IBs, supporting the idea that IBs are the replicative sites of the HMPV genome (Fig. 4, top). To our knowledge, this is the first demonstration of the presence of both species of RNAs in inclusion bodies for HMPV or any member of the related *Paramyxoviridae* family. Interestingly, while the signal for vRNA was mostly in IBs (Fig. 4, white arrowhead) and assembly sites (Fig. 4, top, red arrowhead), the signal for HMPV +RNA was found in IBs but was also dispersed across the cell cytoplasm and not colocalized with the vRNA signal. Since the full-length cRNA serves as a template for the replication of vRNA, the +RNA signal present in IBs could correspond to a mixture of cRNA and viral mRNAs. The cytosolic +RNA signal, in contrast, could correspond exclusively to viral mRNAs. Using fluorescently labeled oligo(dT) probes, the presence of polyadenylated RNAs colocalized with the +RNA was detected in IBs (Fig. 4, blue arrowhead). Although the positive signal from this probe

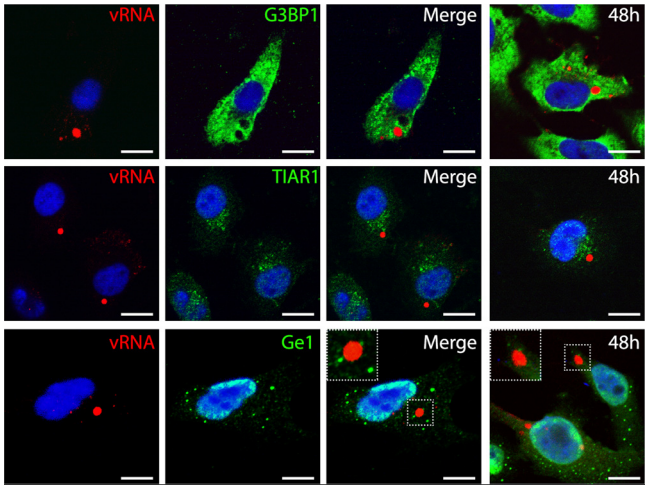

FIG 5 Inclusion bodies do not colocalize with stress granule or P-body markers. BEAS-2B cells were infected with HMPV CAN97-83 at an MOI of 3 PFU/cell and fixed at 24 (left panels) or 48 hpi. FISH and immunofluorescence were performed to detect vRNA (red) and the SG markers G3BP1 and TIAR-1 (green) or P-body marker Ge-1 (green). (Insets) Enlarged images of the small squares with dotted outlines. Bars, 10 μm.

could result from the presence of cellular mRNAs within IBs, the intense colocalization with the +RNA signal strongly suggests the presence of viral mRNAs in IBs. In accord with this possibility, a recent report of a study using mRNA labeling with 5-bromouridine-5′-triphosphate found that VSV mRNAs are synthesized in inclusion bodies and then transported to the cytoplasm of infected cells for translation (20). The phosphoprotein, an essential cofactor of the viral RNA polymerase and nucleocapsid, was also found to form part of the inclusion bodies, colocalizing with the vRNA and +RNA signals (Fig. 4, pink arrowhead). Interestingly, HMPV P and vRNA signals were also found colocalized at putative viral assembly sites (Fig. 4, yellow arrowhead), in agreement with our previous report showing an important role of P in virus assembly (34). The colocalization of the vRNA, +RNA, poly(A), N, and P signals strongly suggests that IBs are the sites of active viral replication and transcription. In contrast, no colocalized signal of the matrix (M) or fusion (F) protein with vRNA in inclusion bodies was detected (Fig. 4, bottom). The HMPV M and F proteins play important roles in the assembly and budding of new particles, but a role in replication has not been reported.

Inclusion bodies are distinct from other cytoplasmic granules. Recent advancements have provided a detailed description of different types of cytoplasmic granules, including stress granules (SGs) and processing bodies (P bodies), and their interactions with viruses (35). For example, RABV Negri bodies have been shown to be in close contact with SGs, with the exchange of viral mRNAs between both organelles being detected (36). For pneumoviruses, conflicting results regarding SG formation upon RSV infection have been obtained. Induction of SG formation as a mechanism of efficient viral replication has been reported by Lindquist et al. (31). In contrast, Hanley et al. showed that wild-type (WT) RSV does not induce the formation of SGs, while a mutant of RSV does (37). To identify a possible interaction between HMPV IBs and stress granules, the colocalization of IBs with the SG markers Ras GTPase-activating protein-binding 1 (G3BP1) and T-cell intracellular antigen-related protein 1 (TIAR-1) was analyzed. No colocalization of vRNA in IBs with SG markers was found at 24 or 48 hpi, demonstrating that IBs and SGs are different cytoplasmic structures. Moreover, G3BP1 and TIAR-1 remained as cytosolic diffuse signals in infected cells, indicating that no induction of SG formation due to HMPV infection was observed at these times postinfection (Fig. 5). P bodies, which are a type of granule involved in different posttranscriptional processes, also did not colocalize with HMPV IBs at 24 or 48 hpi, although some P bodies were occasionally observed in close proximity to these IB sites

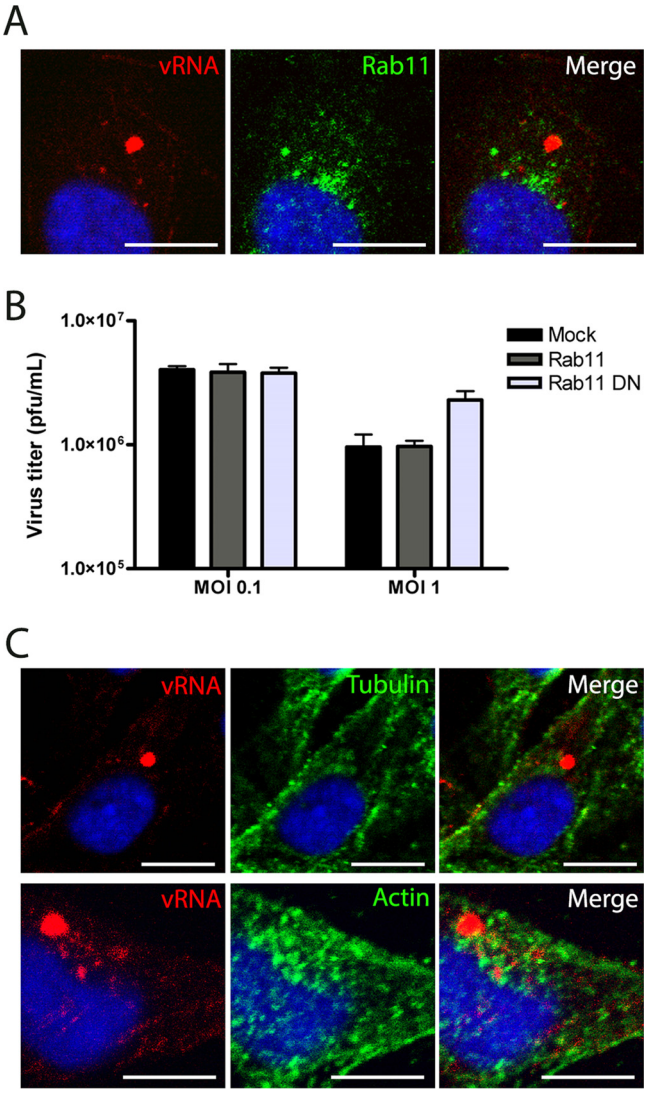

FIG 6 Rab11, β-tubulin, and actin do not colocalize in IBs. (A) BEAS-2B cells were infected with HMPV CAN97-83 at an MOI of 3 PFU/cell and fixed at 24 hpi. FISH and immunofluorescence were performed to detect vRNA (red) and Rab11 (green). Bars, 10 μm. (B) Vero cells were transfected to express GFP-Rab11 or GFP-Rab11 DN. At 24 h posttransfection, the cells were infected with HMPV CAN97-83 at different MOIs (in numbers of PFU per cell). Virus titers were calculated at 72 hpi. (C) BEAS-2B cells were infected with HMPV CAN97-83 at an MOI of 3 PFU/cell and fixed at 24 hpi. FISH and immunofluorescence were performed to detect vRNA (red) and tubulin or β-actin (green). Bars, 10 μm.

(Fig. 5, insets). The biological significance of this interaction warrants future research. Altogether, our results demonstrate that IBs represent independent cytoplasmic sites distinct from SGs or P bodies.

RNA trafficking from IBs does not depend on Rab11$^+$ vesicles or tubulin. Rab GTPases are involved in the cellular sorting of different molecules using vesicular compartments (38). Specifically, Rab11-positive (Rab11$^+$) vesicles were implicated in the movement of Sendai, measles, and influenza virus nucleocapsids through intracellular compartments (39–41). To determine whether Rab11 is involved in the transport of HMPV vRNA from IBs, FISH combined with immunofluorescence was performed. No colocalization between vRNA and Rab11 compartments was found at 24 hpi in IBs or other sites (Fig. 6A). In line with this finding, overexpression of Rab11 or the Rab11 dominant negative (DN) S25N in Vero cells had no significant effect on virus titers (Fig. 6B), in contrast to a previously reported effect of transiently transfected Rab11 on influenza virus growth (42). This result suggests that Rab11 compartments do not have

a role in the transportation of HMPV nucleocapsids from IBs. In a study described in a previous report, we demonstrated a major role of the actin cytoskeleton, but not microtubules, in the assembly and spread of HMPV (34). Therefore, we assessed the colocalization of tubulin and actin with vRNA in IBs and assembly sites. Neither tubulin nor actin was found to be part of IBs. The colocalization of vRNA with microtubules was found to be undetectable in sites outside IBs (Fig. 6C). A colocalization signal for vRNA and actin, though minor, was detectable in sites outside IBs, suggesting the use of the actin cytoskeleton for the transport of HMPV nucleocapsids.

Time course of infection. Our previous experiments demonstrated that HMPV induces the formation of low numbers of IBs in infected cells, even at high MOIs. We speculated that an initial infecting particle could prevent the entry of subsequent particles, thus explaining this phenomenon. Alternatively, multiple replicative sites could converge into fewer IBs for genome replication, as recently reported for human PIV3 (hPIV3) and RABV (43, 44). To distinguish between these options, the formation of IBs from very early times postinfection was analyzed. Protocols of infection with HMPV usually suggest a 3-h period of incubation with cells for virus adsorption. To confirm that this time was sufficient for particle internalization, infected BEAS-2B cells were immediately imaged after adsorption (0 hpi) using Z-stack analysis. Actively replicating sites were observed at 0 hpi, as multiple vRNA/+RNA signal spots were detected (Fig. 7, red arrowheads). The high number of replicative sites detected compared to the MOI used is in agreement with a previous report demonstrating high ratios of internalized HMPV particles/cell during infection using low MOIs (13). Some initial sites were shown to be engaged not only in transcription and/or replication but also in the synthesis of the viral P protein (Fig. 7, blue arrowheads). The fact that multiple replicative sites were detected suggests that the first internalized particles did not prevent the entry of subsequent particles. By 3 hpi, multiple replicative sites containing vRNA/+RNA (Fig. 7, white arrowheads), along with the presence of the +RNA signal dispersed across the cell cytoplasm, were detected. Protein expression was usually associated with viral replicative sites, but it was also dispersed across the cell cytoplasm, as this started to become populated with the +RNA signal. By 6 hpi, replicative sites were closer to cell nuclei and slightly larger (Fig. 7, white arrowheads), potentially as a result of increased RNA synthesis at this time postinfection. The phosphoprotein signal was, as expected, closely associated with each of the replicative sites, but it was also found in cellular extensions maturing from the cell body (Fig. 7, pink arrowheads). Intercellular extensions and viral filaments in infected cells were previously reported to be induced by HMPV as a mechanism for direct cell-to-cell spread (34). The +RNA signal was also found to be dispersed across the cell cytoplasm, which, together with the abundant synthesis of viral protein, reinforces the idea that this signal could correspond to viral mRNAs being transcribed by free ribosomes. Interestingly, at 6 hpi some +RNA signal was also detected on the intercellular extensions (Fig. 7, pink arrowheads). By 12 hpi, larger replicative sites where the signal of vRNA strongly colocalized with the signal of +RNA were visible at the perinuclear area, forming larger IBs (Fig. 7, white arrowheads). The cells at this point were likely engaged in particle assembly (Fig. 7, pink arrowheads). By 24 hpi, a small number of IBs, as well as an increase in their size and proximity to cell nuclei, was evident (Fig. 7, white arrowhead). At this time postinfection, the vRNA and +RNA signals colocalized only in IBs, probably representing the only site in the cell where replication and transcription remained active. The vRNA signal was present in assembly sites (Fig. 7, pink arrowheads), which suggests active transport from IBs, while some signal for +RNA remained dispersed across the cell cytoplasm. Our results strongly suggest that the large inclusion bodies observed by 24 hpi were the result of multiple replicative sites coalescing into fewer inclusion bodies.

Inclusion body coalescence is dependent on actin polymerization. Since the coalescence of replicative sites into larger inclusion bodies appears to be a plausible HMPV replicative strategy, we further examined this process. A recent study reported that the fusion of hPIV3 inclusion bodies was dependent on acetylated α-tubulin

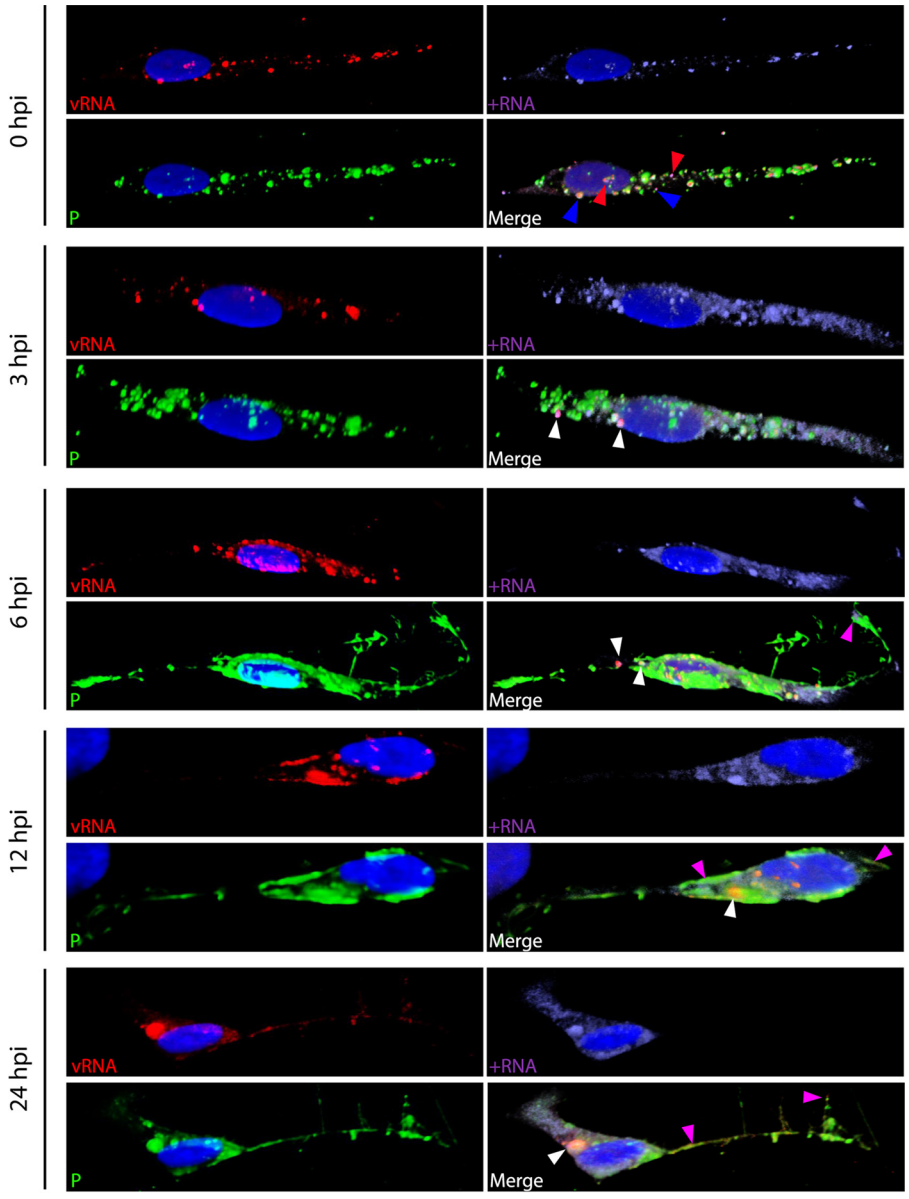

FIG 7 Time course analysis suggests the coalescence of inclusion bodies. BEAS-2B cells were infected with HMPV CAN97-83 at an MOI of 3 PFU/cell and fixed at 0 (3 h postinoculation), 3, 6, 12, and 24 hpi. FISH and immunofluorescence were performed to detect vRNA (red), +RNA (purple), the HMPV P protein (green), and nuclei (blue). Z-stack analysis was performed at every time postinfection.

through a direct interaction with the N-P complex (43). Interestingly, the authors did not find an interaction between acetylated α-tubulin and RSV nucleocapsids. Similarly, α-tubulin was found to not colocalize with HMPV vRNA in our previous experiments. Furthermore, previous data from our lab demonstrated an important role of the actin cytoskeleton, but not microtubules, in the assembly and spread of HMPV; treatment of cells with the actin polymerization inhibitor cytochalasin D negatively impacts viral production (34), but a role of the actin cytoskeleton in inclusion body formation has never been addressed. To determine a putative role of the actin cytoskeleton in the coalescence of inclusion bodies, BEAS-2B cells were infected at an MOI of 3 PFU/cell. After the 3-h adsorption period, by which time infection was previously shown to be established, the cells were incubated with cytochalasin D. The cells were fixed at 3, 6, 12, and 24 hpi, and the numbers of initial replicative sites and inclusion bodies were counted at each time postinfection. As an example, by 24 hpi the infected cells under

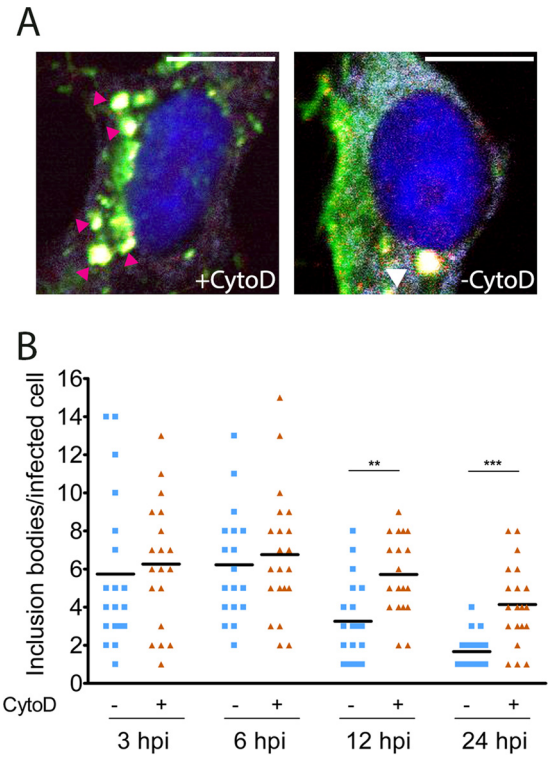

FIG 8 Actin polymerization is involved in inclusion body coalescence. (A) BEAS-2B cells were infected with HMPV CAN97-83 at an MOI of 3 PFU/cell, and at 3 h postinoculation, the cells were treated with DMSO or incubated with 2 μM cytochalasin D (CytoD) until 24 hpi. FISH and immunofluorescence were performed to detect vRNA (red), +RNA (purple), and the HMPV P protein (green). (B) The number of vRNA/+RNA replicative spots in at least 15 DMSO- or cytochalasin D-treated infected cells was counted at each time postinfection. Student's *t* test was performed for statistical analysis. **, $P < 0.001$; ***, $P < 0.0001$. Black bars indicate the average number of inclusion bodies per infected cell.

cytochalasin D treatment presented a higher number of IBs (Fig. 8A, pink arrowheads), which appeared smaller than the IBs in dimethyl sulfoxide (DMSO)-treated cells (Fig. 8A, white arrowhead). The counting of IBs in at least 15 infected cells per condition resulted in two significant discoveries. In line with our previous observations, the number of replicative sites decreased at early times postinfection, suggesting their coalescence for the formation of IBs by 24 hpi. Additionally, the disruption of actin polymerization led to a less dramatic decrease in the number of IBs in time than that in DMSO-treated cells (Fig. 8B). These results suggest that the coalescence of IBs is at least partially dependent on actin cytoskeleton polymerization.

To determine what effect the disruption of IB coalescence had on the transcription and replication of the HMPV genome, a quantitative time course analysis of mRNA and vRNA expression in infected cells was performed. From time zero, an increase in mRNA relative expression was evident, with a peak occurring at 12 hpi, after which mRNA synthesis decreased (Fig. 9A). Cytochalasin D treatment did not significantly affect mRNA expression at very early times postinfection, but a significant decrease was observed at 12 hpi compared to the level of mRNA expression in DMSO-treated control cells. Treatment of cells with nocodazole had no significant effect on mRNA synthesis at any of the times postinfection analyzed. A similar trend was observed when the relative vRNA levels were measured. No significant differences between the DMSO and cytochalasin D treatment conditions were observed by 0, 3, and 6 hpi, but a significant decrease in replication was observed by 12 hpi. Again, addition of nocodazole did not have a significant effect on vRNA synthesis (Fig. 9B). Interestingly, our results indicate that the exponential phase of viral RNA transcription and replication occurs at between 6 and 12 hpi, which coincides with the phase of putative inclusion body coalescence

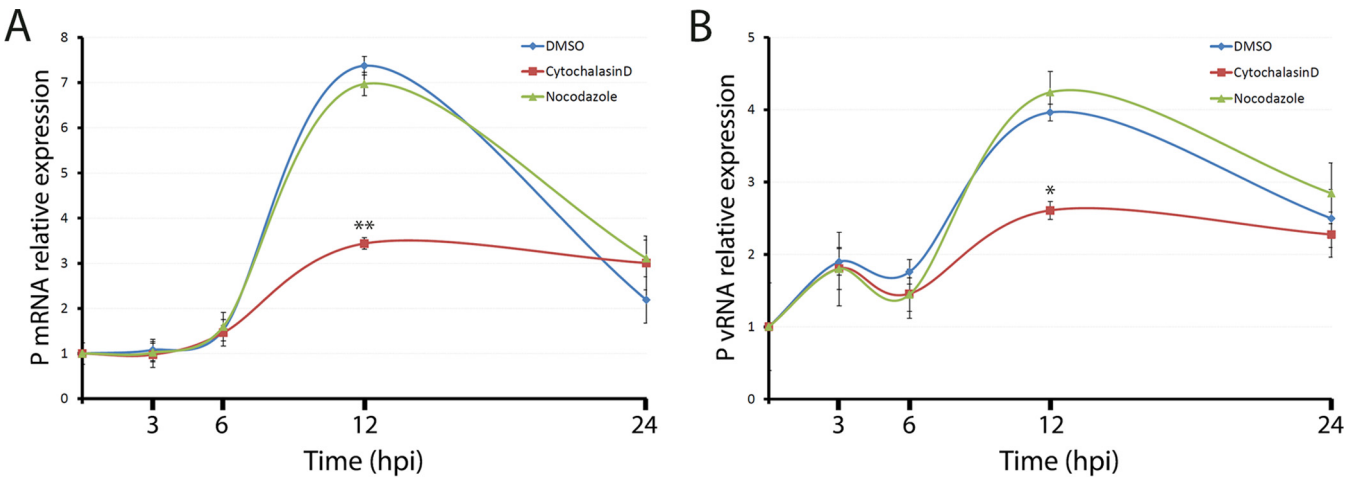

FIG 9 Quantitative time course analysis of HMPV transcription and replication. BEAS-2B cells were infected with HMPV CAN97-83 at an MOI of 3 PFU/cell, and at 3 h postinoculation, the cells were treated with DMSO or incubated with 2 μM cytochalasin D or 17 μM nocodazole until 24 hpi. At each time postinfection, total RNA was extracted from the cells and then quantitative RT-PCR was performed to detect P mRNA (A) or vRNA (B). The levels of expression shown are relative to GAPDH expression levels. Experiments were performed in triplicate. Student's *t* test was performed for statistical analysis. **, $P < 0.001$; *, $P < 0.01$.

(Fig. 8). Altogether, our results strongly suggest that IB coalescence is important for efficient HMPV genome transcription and replication.

DISCUSSION

HMPV is an important human pathogen that can infect people of all ages, with lifetime reinfections and coinfections with RSV being common features (45, 46). Much progress in the understanding of HMPV entry has been made since this pathogen was discovered in 2001. However, HMPV replication and transcription remain less understood. Here, a spatiotemporal analysis of HMPV replication and transcription was performed. To our knowledge, this is the first study to image HMPV genome replication and one of the very few to image the genome replication of paramyxo- or pneumoviruses. To achieve detection of HMPV genomic and antigenomic RNAs, a FISH strategy similar to that used for imaging the replication of influenza and hepatitis C viruses was used (47, 48). The use of multiple labeled probes complementary to a viral RNA target theoretically increases sensitivity up to the level of single molecules. Thus, we have succeeded in imaging HMPV replication beginning at very early times postinfection. Interestingly, the HMPV strategy for replication and transcription involves the formation of a reduced number of IBs, which are always located in the cell cytoplasm, usually within a distance of 5 μm from the nucleus. This strategy differs drastically from that of influenza and hepatitis C virus replication and transcription, which were shown to occur at multiple small replicative sites dispersed across the cell nuclei or cytoplasm (47, 48). Nevertheless, the formation of IBs for replication seems to be a common strategy among NNS viruses. For RABV, a feature of infection is the formation of Negri bodies in the cytoplasm of neurons (18). Although the formation of cytoplasmic inclusion bodies upon rabies virus infection was reported long ago, the demonstration of the presence of the viral genome, antigenome, and mRNAs associated with these structures is much more recent (19). Initially, rabies virus-induced Negri bodies are not surrounded by a membrane but membranes from the RER are recruited around the body at later times postinfection (19, 44, 49). This is in contrast to the inclusion bodies formed by paramyxoviruses, which have been described to be non-membrane surrounded (25–27). This observation raises the question of how, in the absence of surrounding membranes, IBs maintain their architecture. We hypothesize, in light of our observations, that HMPV P and N proteins, most likely associated with cellular components, can form a ring structure surrounding the IB that maintains its architecture while being dynamic enough for efficient RNA synthesis and export. In this context, we hypothesize that the HMPV P protein could have a crucial role, as it has been shown to be closely

associated with actin and has a dual function in viral replication and assembly/spread (34, 50). The HMPV P protein has been reported to homotetramerize, to have regions of intrinsic disorder, and to interact with the N protein (8, 51, 52). Future work will further characterize other cellular components with which the P protein interacts and also determine whether membrane-associated proteins are recruited to HMPV IBs, as is the case for Marburg virus (53). Indeed, Marburg virus inclusion bodies, though not surrounded by a membrane, recruit membranous structures, such as vesicles and multivesicular bodies (53), something not reported for pneumoviruses to date.

Different cytoplasmic non-membrane-surrounded granules have been extensively studied over the past few years. One example is stress granules, which are dense cytosolic structures where stalled preinitiation complexes are accumulated under cellular stress. Many viruses from different families have been reported to manipulate SG formation during infection (54). A recent report showed that RSV, closely related to HMPV, induces the formation of SGs for efficient replication (31). The number of IBs in cells with SGs was shown to increase by approximately 5-fold compared to the number in cells without SGs (31). These results differ from ours in at least two ways. First, the number of HMPV IBs never exceeded 7 per infected cell, independent of the MOI or the time postinfection, whereas up to 100 IBs were reported for RSV. Second, no obvious induction of SG formation was detected upon HMPV infection by 24 or 48 hpi. In agreement with our results, Hanley et al. did not observe SG formation upon infection using WT RSV (37). Furthermore, the replication of HMPV also seems to be similar to that of the paramyxovirus PIV5. For this virus, the formation of low numbers of cytoplasmic IBs was revealed to be a strategy to circumvent the IFN response (33). Moreover, PIV5 cytoplasmic bodies were shown to be different from SGs, autophagosomes, and P bodies. In this context, the formation of IBs by NNS viruses might represent a novel strategy to subvert innate immune responses. For example, Ebola virus was shown to sequester SG components within IBs, a process that helps the virus to hinder the formation of SGs in infected cells (55). In addition, P bodies, another group of cytosolic granules that play a role in different RNA posttranscriptional processes, such as mRNA decay and microRNA-induced mRNA silencing, were also studied in this work. Interestingly, P bodies were sometimes found in close proximity to IBs in HMPV-infected cells. Considering that P bodies are a processing station for mRNA and that we suggest that HMPV IBs contain a large amount of viral mRNAs, a flow of molecules between both organelles is possible. Future research will allow us to further address this hypothesis.

A recent report indicates that HMPV entry via endocytosis is a process that takes up to 2 h, with some viral particles quickly entering and others entering much more slowly (13). After fusion with the endosomal membranes, particles are released into the cytoplasm, but what happens after release was unknown. Our results show that after 3 h of viral adsorption (defined by us as 0 hpi), multiple sites actively involved in the replication/transcription and translation of viral proteins are present in the cytoplasm. Each of those multiple replicative sites could correspond to initial incoming particles, arguing against a restriction in the entry of subsequent particles, which coincides with what was reported by Cox et al. (13). Furthermore, our results showed that from 6 hpi to 24 hpi, replicative sites significantly decreased in number and increased in size, suggesting their coalescence to give rise to inclusion bodies. This process was shown to be affected by actin polymerization, but not microtubules. To our knowledge, a role for actin polymerization in the early coalescence of replicative sites has not been previously reported for pneumoviruses. A very recent report demonstrated that the fusion of hPIV3 inclusion bodies occurred after 6 hpi and that it was dependent on acetylated α-tubulin (43). Acetylated α-tubulin was shown to directly interact with the hPIV3 N-P complex but did not interact with the RSV N-P complex. It is possible that the RSV N-P complex, similarly to the HMPV N-P complex, interacts mainly with actin and/or actin-related proteins. Our observations at early times postinfection, at which the presence of the P protein was found to be associated with replicative sites, further support this hypothesis. In agreement with this, disruption of actin polymerization was

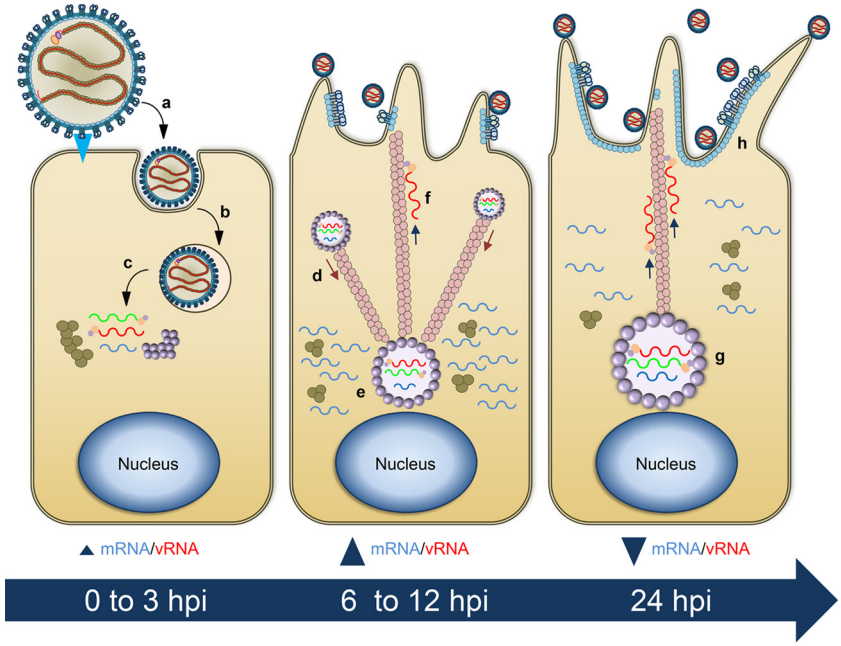

FIG 10 Proposed events of HMPV transcription and replication. After attachment and endocytosis (a), viral nucleocapsids are released into the cell cytoplasm (b). Incoming particles can give rise to replicative sites (c), where vRNA (red), cRNA (green), mRNAs (blue), and viral proteins are readily synthesized. At between 6 and 12 hpi, replicative sites are more compact and start to coalesce (d) into larger inclusion bodies located close to cell nuclei (e). The synthesis of mRNA and vRNA is exponential at these times postinfection. From inclusion bodies, vRNA might be transported to assembly sites (f) through the actin cytoskeleton. The cell cytoplasm is populated by viral mRNAs. By 24 hpi, large inclusion bodies are visible at the perinuclear area (g). At this and later times postinfection, IBs remain as the only sites where transcription and replication are still active. At this point, cells are engaged in particle assembly and spread (h). Light blue circles, matrix protein; brown circles, nucleoprotein; purple circles, phosphoprotein.

shown to result in fragmentation of RABV Negri bodies (44). Furthermore, fusion of Negri bodies was suggested to be an intrinsic characteristic of these organelles, as they have a viscous liquid nature (44).

Once HMPV IBs were established close to cell nuclei by 12 hpi, they remained as active sites where vRNA, +RNA, and mRNA could be found, with the synthesis of viral proteins occurring nearby (Fig. 10). As HMPV IBs gave a positive signal for N and P proteins but not for the M and F assembly proteins, we conclude that IBs represent sites exclusively for transcription and replication of the genome. In previous work, we demonstrated that by 12 hpi, viral particles are actively being released from infected BEAS-2B cells (34). It is feasible that nucleocapsid formation occurs within IBs and from there they are transported via the actin cytoskeleton (34) to assembly sites on the plasma membrane through a process similar to that in filoviruses (23, 24, 56). An interesting study demonstrated that newly synthesized VSV mRNAs were transported through microtubules from IBs to the cell cytoplasm, so they may be translated by free ribosomes (20). In our experiments, a signal of +RNA (not colocalized with vRNA or nucleoprotein) was observed to be dispersed across the cell cytoplasm from very early times postinfection, which we suggest is the result of an active transport of HMPV mRNAs from IBs. As no effect of nocodazole on HMPV transcription or IB coalescence was observed, a role for microtubules in these processes is unlikely. Our results rather suggest an important role of the actin cytoskeleton in mRNA transcription, which we suggest is due to a reduction in the coalescence of inclusion bodies. The exponential synthesis of mRNA and vRNA between 6 and 12 hpi correlates well with the phase of putative coalescence of replicative sites, therefore implicating IB coalescence in replication and transcription efficiency. Nevertheless, we cannot discard the possibility of other additional roles beyond IB coalescence that the actin cytoskeleton could play. Among those is the export of mRNAs into the cell cytoplasm, which would affect the

synthesis of essential replicative proteins, including the viral polymerase. Interestingly, mRNA and vRNA synthesis was found to be exponential from 6 hpi to at least 12 hpi, which would argue against the hypothesis of a viral polymerase shift from a transcriptional mode to a replication mode. Rather, our results suggest the coexistence of different populations of nucleocapsids committed to either replication or transcription of the viral genome.

The present work represents an advancement in our understanding of the biology of HMPV IB formation and function, which also has important clinical implications. For example, as coinfections with HMPV and other respiratory viruses are common, the question of how IB formation would operate in the presence of different viral genomes remains open. Furthermore, it has been shown that PIV5 IBs can remain quiescent in cells for years (57). Thus, considering the high sensitivity and specificity of the techniques employed in this work, the exploration of HMPV RNA quiescence in respiratory tissues could be exciting.

MATERIALS AND METHODS

Cell lines. BEAS-2B human bronchial epithelial cells, obtained from ATCC, were grown in bronchial epithelial cell growth medium (BEBM) supplemented with the reagents from a BEGM SingleQuot kit and growth factors (Lonza). BSR cells, which stably express the T7 RNA polymerase (a kind gift of Klaus Konzelmann, University of Munich, Munich, Germany), were grown in Dulbecco's modified Eagle's medium (DMEM; Gibco) supplemented with 10% fetal bovine serum (FBS) and every other week with 500 μg/ml of G-418 (Gibco).

Plasmids, antibodies, and reagents. Plasmids p(+)JPS07E2, pCITE-P, and pCITE-N, harboring the full-length genome, P protein, and N protein of HMPV strain JPS02-76, respectively, were kindly provided by Makoto Takeda (National Institute of Infectious Diseases, Tokyo, Japan). Wild-type Rab11a and Rab11a DN S25N cloned as green fluorescent protein (GFP) N-terminal fusions were a kind gift from Gary Whittaker (Cornell University, Ithaca, NY, USA). Antibodies to detect HMPV N protein (catalog number ab94801), P protein (catalog number ab94803), and F protein (catalog number ab94800) were obtained from Abcam. Detection of HMPV M was achieved using a polyclonal antibody against the avian metapneumovirus M protein, kindly provided by Sagar M. Goyal (University of Minnesota, MN, USA). Antibodies for detection of Rab11 (antibody D4F5) and β-actin (antibody 13E5) were purchased from Cell Signaling. Antibody for detection of α-tubulin (antibody 66031) was obtained from the Proteintech Group. Antibodies for detection of G3BP1 (Proteintech antibody 13057-2-AP), TIAR-1 (antibody sc-1751), and Ge-1 (antibody sc-8418) were kindly provided by Jozsef Gal from the University of Kentucky. Secondary antibodies conjugated with fluorescein isothiocyanate (FITC), tetramethyl rhodamine isothiocyanate (TRITC), or Alexa Fluor 647 were obtained from Jackson ImmunoResearch. Cytochalasin D was purchased from Sigma (catalog number C8273). Nocodazole was purchased from Calbiochem (catalog number 487928).

Virus propagation and infection. WT HMPV strain CAN97-83 (a kind gift of Guy Boivin, Université Laval, Canada) and recombinant, GFP-expressing HMPV (rgHMPV) strain CAN97-83 (a kind gift of Peter Collins and Ursula Buchholz, NIH, USA) were propagated and the titers in Vero cells were determined as previously described (34). WT HMPV strains TN9332 and TN91316 were kindly provided by John Williams (University of Pittsburgh, Pittsburgh, PA, USA) and also propagated in Vero cells.

FISH. Two sets of probes, based on the sequence of HMPV prototype strain CAN97-83, were designed to detect HMPV vRNA or HMPV +RNA. Each set was composed of 48 DNA probes which target the HMPV RNA sequence between nucleotides (nt) 1 and 5467 (containing the genes for N, P, M, F, and M2) and were obtained from Biosearch Technologies (Novato, CA). Each probe was 20 nt long and linked at the 3′ end to the Quasar 570 fluorophore for probes complementary to vRNA and linked to the Quasar 670 fluorophore for probes complementary to +RNA. Probes were designed using the software provided by the company. In cases in which the probes had an overlapping target on the sequence (and were therefore complementary), we manually corrected the sequence such that none of the probes of one set were complementary to probes of the other set. For the fluorescence *in situ* hybridization (FISH) experiments, BEAS-2B cells grown on 10-mm precoated coverslips (precoated with 0.01 mg/ml fibronectin, 0.03 mg/ml bovine collagen type I, and 0.01 mg/ml bovine serum albumin in BEBM) were infected with HMPV at the MOI indicated above and in the figure legends. At different times postinfection, cells were fixed for 10 min with 4% paraformaldehyde (PFA) and then permeabilized overnight with 70% ethanol at 4°C. On the next day, the cells were washed once with 2× SSC (0.3 M NaCl and 0.03 M sodium citrate, pH 7.0.)–10% formamide buffer and then incubated overnight at 25°C in hybridization buffer (4× SSC, 1× Denhardt's solution, 150 μg/ml single-stranded DNA, 2 mM EDTA, 50% formamide, and 10% dextran sulfate in diethyl pyrocarbonate-treated water) containing the probes at a final concentration of 2.5 mM. After 24 h, the cells were washed two times for 20 min each time with 2× SSC–10% formamide buffer, and the slides were then mounted using Vectashield mounting medium (Vector Laboratories, Burlingame, CA). Oligo(dT) probes linked at the 3′ end to the Quasar 570 fluorophore were also obtained from Biosearch Technologies (Novato, CA) and used at a final concentration of 5 mM. Pictures were taken using a Nikon 1A confocal microscope and analyzed with NIS-Elements software and ImageJ Fiji software.

For experiments in which a combination of FISH and immunofluorescence techniques was performed, FISH was done first followed by immunofluorescence, avoiding the Triton X-100 permeabilization step.

Immunofluorescence experiments. BSR cells grown in 8-well chamber slides (Thermo Fisher) were transfected with the plasmids indicated above using the Lipofectamine 2000 reagent following the manufacturer's guidelines (Invitrogen). At the times posttransfection indicated above, cells were processed for FISH and immunofluorescence. BEAS-2B cells grown on 10-mm precoated coverslips were infected with HMPV, and at the times postinfection indicated above, cells were washed in phosphate-buffered saline (PBS) and fixed with 4% PFA for 15 min at room temperature. The cells were then permeabilized in 1% Triton X-100 for 15 min at 4°C, followed by blocking in 1% normal goat serum and incubation with the corresponding primary antibody overnight at 4°C. On the following day, the cells were washed seven times with 0.05% Tween 20–PBS and incubated at 4°C with secondary antibodies for 1 h. The coverslips were then mounted on glass slides using Vectashield mounting medium. Pictures were taken using a Nikon 1A confocal microscope and analyzed with NIS-Elements software and ImageJ Fiji software. Some images were processed with Adobe Photoshop software, with equivalent adjustments being made to all panels.

RNA extraction and quantitative RT-PCR. BEAS-2B cells grown in 12-well plates were infected at an MOI of 3 PFU/cell in triplicate. At each time postinfection indicated above, the cells were washed twice with PBS and lysed with 500 μl of TriPure isolation reagent (Sigma), and total RNA was extracted according to the manufacturer's instructions. RNA was subsequently treated with amplification-grade DNase I (Sigma) for 15 min at room temperature, followed by inactivation at 70°C for 10 min. Reverse transcription was performed starting with 500 ng of DNase-treated RNA, 1.25 mM deoxynucleoside triphosphates, 10 U avian myeloblastosis virus reverse transcriptase (Promega), and 1.25 μM an oligo(dT)$_{20}$-specific primer (for mRNA amplification) or primer 5′-AACGCGTATAAATTAAGTTAC-3′ (for vRNA amplification). The reaction mixtures were incubated at 80°C for 10 min and then at 42°C for 60 min. For quantitative PCR, 2 μl of freshly made cDNA was mixed with 1.25 μM each specific primers Pfw (5′-ACATTGCTACAGCAGGACCC-3′) and Prv (5′-CACCACTTGTGCTCTCGTCT-3′), Perfecta SYBR green Supermix, and low-carboxy-X-rhodamine reagent (Quanta Biosciences) according to the manufacturer's instructions. All assays were performed in triplicate in a Stratagene Mx 3005P system (Agilent Technologies). Cycle parameters were as follows: 95°C for 2 min and 40 cycles of 95°C for 30 s, 55°C for 30 s, and 72°C for 60 s. RNA extractions were performed in triplicate, and results were normalized to the average level of expression of the housekeeping gene control, glyceraldehyde-3-phosphate dehydrogenase (GAPDH).

Statistical analysis. The average value and standard deviation from the indicated experiments were calculated, and the Student *t* test was performed for statistical evaluation. *P* values are indicated for each individual experiment. All statistical analyses were performed using GraphPad Prism software.

ACKNOWLEDGMENTS

We thank the members of the R. E. Dutch lab for careful readings of the manuscript. Our acknowledgments also go to Carole Moncman for her valuable advice with the confocal microscopy.

REFERENCES

1. Pelletier G, Dery P, Abed Y, Boivin G. 2002. Respiratory tract reinfections by the new human metapneumovirus in an immunocompromised child. Emerg Infect Dis 8:976–978. https://doi.org/10.3201/eid0809.020238.
2. van den Hoogen BG, de Jong JC, Groen J, Kuiken T, de Groot R, Fouchier RA, Osterhaus AD. 2001. A newly discovered human pneumovirus isolated from young children with respiratory tract disease. Nat Med 7:719–724. https://doi.org/10.1038/89098.
3. Widmer K, Zhu Y, Williams JV, Griffin MR, Edwards KM, Talbot HK. 2012. Rates of hospitalizations for respiratory syncytial virus, human metapneumovirus, and influenza virus in older adults. J Infect Dis 206:56–62. https://doi.org/10.1093/infdis/jis309.
4. Boivin G, Abed Y, Pelletier G, Ruel L, Moisan D, Cote S, Peret TC, Erdman DD, Anderson LJ. 2002. Virological features and clinical manifestations associated with human metapneumovirus: a new paramyxovirus responsible for acute respiratory-tract infections in all age groups. J Infect Dis 186:1330–1334. https://doi.org/10.1086/344319.
5. Afonso CL, Amarasinghe GK, Banyai K, Bao Y, Basler CF, Bavari S, Bejerman N, Blasdell KR, Briand FX, Briese T, Bukreyev A, Calisher CH, Chandran K, Cheng J, Clawson AN, Collins PL, Dietzgen RG, Dolnik O, Domier LL, Durrwald R, Dye JM, Easton AJ, Ebihara H, Farkas SL, Freitas-Astua J, Formenty P, Fouchier RA, Fu Y, Ghedin E, Goodin MM, Hewson R, Horie M, Hyndman TH, Jiang D, Kitajima EW, Kobinger GP, Kondo H, Kurath G, Lamb RA, Lenardon S, Leroy EM, Li CX, Lin XD, Liu L, Longdon B, Marton S, Maisner A, Muhlberger E, Netesov SV, Nowotny N, et al. 2016. Taxonomy of the order Mononegavirales: update 2016. Arch Virol 161:2351–2360. https://doi.org/10.1007/s00705-016-2880-1.
6. van den Hoogen BG, van Doornum GJ, Fockens JC, Cornelissen JJ, Beyer WE, de Groot R, Osterhaus AD, Fouchier RA. 2003. Prevalence and clinical symptoms of human metapneumovirus infection in hospitalized patients. J Infect Dis 188:1571–1577. https://doi.org/10.1086/379200.
7. Ruigrok RW, Crepin T, Kolakofsky D. 2011. Nucleoproteins and nucleocapsids of negative-strand RNA viruses. Curr Opin Microbiol 14:504–510. https://doi.org/10.1016/j.mib.2011.07.011.
8. Derdowski A, Peters TR, Glover N, Qian R, Utley TJ, Burnett A, Williams JV, Spearman P, Crowe JE, Jr. 2008. Human metapneumovirus nucleoprotein and phosphoprotein interact and provide the minimal requirements for inclusion body formation. J Gen Virol 89:2698–2708. https://doi.org/10.1099/vir.0.2008/004051-0.
9. Leyrat C, Renner M, Harlos K, Huiskonen JT, Grimes JM. 2014. Drastic changes in conformational dynamics of the antiterminator M2-1 regulate transcription efficiency in Pneumovirinae. Elife 3:e02674. https://doi.org/10.7554/eLife.02674.
10. Khattar SK, Yunus AS, Samal SK. 2001. Mapping the domains on the phosphoprotein of bovine respiratory syncytial virus required for N-P and P-L interactions using a minigenome system. J Gen Virol 82:775–779. https://doi.org/10.1099/0022-1317-82-4-775.
11. Renner M, Bertinelli M, Leyrat C, Paesen GC, Saraiva de Oliveira LF, Huiskonen JT, Grimes JM. 2016. Nucleocapsid assembly in pneumoviruses is regulated by conformational switching of the N protein. Elife 5:e12627. https://doi.org/10.7554/eLife.12627.
12. Lamb RA, Mahy BW, Choppin PW. 1976. The synthesis of Sendai virus polypeptides in infected cells. Virology 69:116–131. https://doi.org/10.1016/0042-6822(76)90199-9.
13. Cox RG, Mainou BA, Johnson M, Hastings AK, Schuster JE, Dermody TS,

Williams JV. 2015. Human metapneumovirus is capable of entering cells by fusion with endosomal membranes. PLoS Pathog 11:e1005303. https://doi.org/10.1371/journal.ppat.1005303.
14. Chang A, Masante C, Buchholz UJ, Dutch RE. 2012. Human metapneumovirus (HMPV) binding and infection are mediated by interactions between the HMPV fusion protein and heparan sulfate. J Virol 86:3230–3243. https://doi.org/10.1128/JVI.06706-11.
15. Lamb RA, Parks GD. 2013. Paramyxoviridae, p 957–995. *In* Knipe DM, Howley PM, Cohen JI, Griffin DE, Lamb RA, Martin MA, Racaniello VR, Roizman B (ed), Fields virology, 6th ed. Lippincott Williams & Wilkins, Philadelphia, PA.
16. Biacchesi S, Skiadopoulos MH, Boivin G, Hanson CT, Murphy BR, Collins PL, Buchholz UJ. 2003. Genetic diversity between human metapneumovirus subgroups. Virology 315:1–9. https://doi.org/10.1016/S0042-6822(03)00528-2.
17. Noton SL, Fearns R. 2015. Initiation and regulation of paramyxovirus transcription and replication. Virology 479-480:545–554. https://doi.org/10.1016/j.virol.2015.01.014.
18. Matsumoto S. 1962. Electron microscopy of nerve cells infected with street rabies virus. Virology 17:198–202. https://doi.org/10.1016/0042-6822(62)90099-5.
19. Lahaye X, Vidy A, Pomier C, Obiang L, Harper F, Gaudin Y, Blondel D. 2009. Functional characterization of Negri bodies (NBs) in rabies virus-infected cells: evidence that NBs are sites of viral transcription and replication. J Virol 83:7948–7958. https://doi.org/10.1128/JVI.00554-09.
20. Heinrich BS, Cureton DK, Rahmeh AA, Whelan SP. 2010. Protein expression redirects vesicular stomatitis virus RNA synthesis to cytoplasmic inclusions. PLoS Pathog 6:e1000958. https://doi.org/10.1371/journal.ppat.1000958.
21. Becker S, Rinne C, Hofsass U, Klenk HD, Muhlberger E. 1998. Interactions of Marburg virus nucleocapsid proteins. Virology 249:406–417. https://doi.org/10.1006/viro.1998.9328.
22. Kolesnikova L, Muhlberger E, Ryabchikova E, Becker S. 2000. Ultrastructural organization of recombinant Marburg virus nucleoprotein: comparison with Marburg virus inclusions. J Virol 74:3899–3904. https://doi.org/10.1128/JVI.74.8.3899-3904.2000.
23. Schudt G, Dolnik O, Kolesnikova L, Biedenkopf N, Herwig A, Becker S. 2015. Transport of ebolavirus nucleocapsids is dependent on actin polymerization: live-cell imaging analysis of ebolavirus-infected cells. J Infect Dis 212(Suppl 2):S160–S166. https://doi.org/10.1093/infdis/jiv083.
24. Schudt G, Kolesnikova L, Dolnik O, Sodeik B, Becker S. 2013. Live-cell imaging of Marburg virus-infected cells uncovers actin-dependent transport of nucleocapsids over long distances. Proc Natl Acad Sci U S A 110:14402–14407. https://doi.org/10.1073/pnas.1307681110.
25. Compans RW, Holmes KV, Dales S, Choppin PW. 1966. An electron microscopic study of moderate and virulent virus-cell interactions of the parainfluenza virus SV5. Virology 30:411–426. https://doi.org/10.1016/0042-6822(66)90119-X.
26. Nakai T, Shand FL, Howatson AF. 1969. Development of measles virus in vitro. Virology 38:50–67. https://doi.org/10.1016/0042-6822(69)90127-5.
27. Churchill AE. 1963. Intranuclear inclusions produced by bovine parainfluenza. Nature 197:409.
28. Narang HK. 1982. Ultrastructural study of long-term canine distemper virus infection in tissue culture cells. Infect Immun 36:310–319.
29. Norrby E, Marusyk H, Orvell C. 1970. Morphogenesis of respiratory syncytial virus in a green monkey kidney cell line (Vero). J Virol 6:237–242.
30. Garcia J, Garcia-Barreno B, Vivo A, Melero JA. 1993. Cytoplasmic inclusions of respiratory syncytial virus-infected cells: formation of inclusion bodies in transfected cells that coexpress the nucleoprotein, the phosphoprotein, and the 22K protein. Virology 195:243–247. https://doi.org/10.1006/viro.1993.1366.
31. Lindquist ME, Lifland AW, Utley TJ, Santangelo PJ, Crowe JE, Jr. 2010. Respiratory syncytial virus induces host RNA stress granules to facilitate viral replication. J Virol 84:12274–12284. https://doi.org/10.1128/JVI.00260-10.
32. Randall RE, Goodbourn S. 2008. Interferons and viruses: an interplay between induction, signalling, antiviral responses and virus countermeasures. J Gen Virol 89:1–47. https://doi.org/10.1099/vir.0.83391-0.
33. Carlos TS, Young DF, Schneider M, Simas JP, Randall RE. 2009. Parainfluenza virus 5 genomes are located in viral cytoplasmic bodies whilst the virus dismantles the interferon-induced antiviral state of cells. J Gen Virol 90:2147–2156. https://doi.org/10.1099/vir.0.012047-0.
34. El Najjar F, Cifuentes-Munoz N, Chen J, Zhu H, Buchholz UJ, Moncman CL, Dutch RE. 2016. Human metapneumovirus induces reorganization of the actin cytoskeleton for direct cell-to-cell spread. PLoS Pathog 12:e1005922. https://doi.org/10.1371/journal.ppat.1005922.
35. Lloyd RE. 2012. How do viruses interact with stress-associated RNA granules? PLoS Pathog 8:e1002741. https://doi.org/10.1371/journal.ppat.1002741.
36. Nikolic J, Civas A, Lama Z, Lagaudriere-Gesbert C, Blondel D. 2016. Rabies virus infection induces the formation of stress granules closely connected to the viral factories. PLoS Pathog 12:e1005942. https://doi.org/10.1371/journal.ppat.1005942.
37. Hanley LL, McGivern DR, Teng MN, Djang R, Collins PL, Fearns R. 2010. Roles of the respiratory syncytial virus trailer region: effects of mutations on genome production and stress granule formation. Virology 406:241–252. https://doi.org/10.1016/j.virol.2010.07.006.
38. Bhuin T, Roy JK. 2014. Rab proteins: the key regulators of intracellular vesicle transport. Exp Cell Res 328:1–19. https://doi.org/10.1016/j.yexcr.2014.07.027.
39. Chambers R, Takimoto T. 2010. Trafficking of Sendai virus nucleocapsids is mediated by intracellular vesicles. PLoS One 5:e10994. https://doi.org/10.1371/journal.pone.0010994.
40. Amorim MJ, Bruce EA, Read EK, Foeglein A, Mahen R, Stuart AD, Digard P. 2011. A Rab11- and microtubule-dependent mechanism for cytoplasmic transport of influenza A virus viral RNA. J Virol 85:4143–4156. https://doi.org/10.1128/JVI.02606-10.
41. Nakatsu Y, Ma X, Seki F, Suzuki T, Iwasaki M, Yanagi Y, Komase K, Takeda M. 2013. Intracellular transport of the measles virus ribonucleoprotein complex is mediated by Rab11A-positive recycling endosomes and drives virus release from the apical membrane of polarized epithelial cells. J Virol 87:4683–4693. https://doi.org/10.1128/JVI.02189-12.
42. Bruce EA, Digard P, Stuart AD. 2010. The Rab11 pathway is required for influenza A virus budding and filament formation. J Virol 84:5848–5859. https://doi.org/10.1128/JVI.00307-10.
43. Zhang S, Jiang Y, Cheng Q, Zhong Y, Qin Y, Chen M. 2017. Inclusion body fusion of human parainfluenza virus type 3 regulated by acetylated alpha-tubulin enhances viral replication. J Virol 91:e01802-16. https://doi.org/10.1128/JVI.01802-16.
44. Nikolic J, Le Bars R, Lama Z, Scrima N, Lagaudriere-Gesbert C, Gaudin Y, Blondel D. 2017. Negri bodies are viral factories with properties of liquid organelles. Nat Commun 8:58. https://doi.org/10.1038/s41467-017-00102-9.
45. Greensill J, McNamara PS, Dove W, Flanagan B, Smyth RL, Hart CA. 2003. Human metapneumovirus in severe respiratory syncytial virus bronchiolitis. Emerg Infect Dis 9:372–375. https://doi.org/10.3201/eid0903.020289.
46. Semple MG, Cowell A, Dove W, Greensill J, McNamara PS, Halfhide C, Shears P, Smyth RL, Hart CA. 2005. Dual infection of infants by human metapneumovirus and human respiratory syncytial virus is strongly associated with severe bronchiolitis. J Infect Dis 191:382–386. https://doi.org/10.1086/426457.
47. Lakdawala SS, Wu Y, Wawrzusin P, Kabat J, Broadbent AJ, Lamirande EW, Fodor E, Altan-Bonnet N, Shroff H, Subbarao K. 2014. Influenza A virus assembly intermediates fuse in the cytoplasm. PLoS Pathog 10:e1003971. https://doi.org/10.1371/journal.ppat.1003971.
48. Shulla A, Randall G. 2015. Spatiotemporal analysis of hepatitis C virus infection. PLoS Pathog 11:e1004758. https://doi.org/10.1371/journal.ppat.1004758.
49. Matsumoto S, Schneider LG, Kawai A, Yonezawa T. 1974. Further studies on the replication of rabies and rabies-like viruses in organized cultures of mammalian neural tissues. J Virol 14:981–996.
50. Collins PL, Hill MG, Cristina J, Grosfeld H. 1996. Transcription elongation factor of respiratory syncytial virus, a nonsegmented negative-strand RNA virus. Proc Natl Acad Sci U S A 93:81–85. https://doi.org/10.1073/pnas.93.1.81.
51. Curran J, Marq JB, Kolakofsky D. 1995. An N-terminal domain of the Sendai paramyxovirus P protein acts as a chaperone for the NP protein during the nascent chain assembly step of genome replication. J Virol 69:849–855.
52. Leyrat C, Renner M, Harlos K, Grimes JM. 2013. Solution and crystallographic structures of the central region of the phosphoprotein from human metapneumovirus. PLoS One 8:e80371. https://doi.org/10.1371/journal.pone.0080371.
53. Dolnik O, Stevermann L, Kolesnikova L, Becker S. 2015. Marburg virus inclusions: a virus-induced microcompartment and interface to multivesicular bodies and the late endosomal compartment. Eur J Cell Biol 94:323–331. https://doi.org/10.1016/j.ejcb.2015.05.006.
54. Valiente-Echeverria F, Melnychuk L, Mouland AJ. 2012. Viral modulation

of stress granules. Virus Res 169:430–437. https://doi.org/10.1016/j.virusres.2012.06.004.
55. Nelson EV, Schmidt KM, Deflube LR, Doganay S, Banadyga L, Olejnik J, Hume AJ, Ryabchikova E, Ebihara H, Kedersha N, Ha T, Muhlberger E. 2016. Ebola virus does not induce stress granule formation during infection and sequesters stress granule proteins within viral inclusions. J Virol 90:7268–7284. https://doi.org/10.1128/JVI.00459-16.
56. Dolnik O, Kolesnikova L, Welsch S, Strecker T, Schudt G, Becker S. 2014. Interaction with Tsg101 is necessary for the efficient transport and release of nucleocapsids in Marburg virus-infected cells. PLoS Pathog 10:e1004463. https://doi.org/10.1371/journal.ppat.1004463.
57. Fearns R, Young DF, Randall RE. 1994. Evidence that the paramyxovirus simian virus 5 can establish quiescent infections by remaining inactive in cytoplasmic inclusion bodies. J Gen Virol 75(Pt 12):3525–3539. https://doi.org/10.1099/0022-1317-75-12-3525.